frontiers | Frontiers in Marine Science

TYPE Original Research
PUBLISHED 06 February 2023
DOI 10.3389/fmars.2023.1078831



OPEN ACCESS

EDITED BY
Veerle Ann Ida Huvenne,
University of Southampton,
United Kingdom

REVIEWED BY
Francesco Marcello Falcieri,
Department of Earth System Sciences and Technologies for the Environment (CNR),
Italy
Rob Hall,
University of East Anglia, United Kingdom

*CORRESPONDENCE
Lénaïg Brun
lenaig.brun@ifremer.fr

SPECIALTY SECTION
This article was submitted to Deep-Sea Environments and Ecology, a section of the journal Frontiers in Marine Science

RECEIVED 24 October 2022
ACCEPTED 10 January 2023
PUBLISHED 06 February 2023

CITATION
Brun L, Pairaud I, Jacinto RS, Garreau P and Dennielou B (2023) Strong hydrodynamic processes observed in the Mediterranean Cassidaigne submarine canyon. *Front. Mar. Sci.* 10:1078831. doi: 10.3389/fmars.2023.1078831



# Strong hydrodynamic processes observed in the Mediterranean Cassidaigne submarine canyon

Lénaïg Brun[1]*, Ivane Pairaud[1], Ricardo Silva Jacinto[2], Pierre Garreau[1] and Bernard Dennielou[2]

[1]Ifremer, University of Brest, UMR 6523 CNRS, IRD, Laboratoire d'Océanographie Physique et Spatiale, Plouzané, France, [2]Ifremer, Geo-Ocean, University of Brest, CNRS, UMR 6538, Plouzané, France

**Introduction:** Submarine canyons are incisive morphologies that play an important role in the exchange between shallow and deep waters. They interact with the general circulation and induce a specific circulation locally oriented by the morphology. The characteristics of the physical processes at play, the way they interact with each other and the influence of extreme events is still an open question as few observations are available. To answer this question and to improve the representation of submarine canyons in numerical models, it is key to understand the specific circulation patterns and their transitions in these specific environments.

**Methods:** This paper presents observations of currents, temperature and turbidity along the Cassidaigne canyon, northwestern Mediterranean Sea. Two oceanographic cruises carried out in 2017 and 2019 gathered data from the outer shelf and canyon head at 100-400 m depth to the base of the continental slope at 1900 m depth.

**Results and Discussion:** The circulation in the Cassidaigne area is subject to upwelling and downwelling-favorable winds, to the Northern Current and its associated mesoscale structures and is oriented by the local morphology. Upwellings occur both during stratified and non-stratified conditions. They are triggered by a wind forcing higher than 14 m $s^{-1}$ and their consecutive relaxations are marked by a counter-current. Near the canyon head and on the shelf, the current orientation depends on the stratification, the wind, the bottom morphology and the general circulation. The mesoscale variability of the Northern Current can lead to its intrusion over the shelf leading to barotropic cross currents over the canyon. At 1700 m depth, a quasi-permanent residual up-canyon flow is observed in a narrow gorge area and can be extrapolated to the canyon body. Finally, turbidity currents were observed for the first time in connection with upwelling events, suggesting the key role of canyons' internal hydrodynamics on shelf sedimentary processes.

KEYWORDS

**circulation, submarine canyon, Cassidaigne, Mediterranean Sea, upwelling, Northern Current, turbidity current, morphology**

# 1 Introduction

Submarine canyons incising continental slopes constitute key oceanic morphologies favoring the exchange of organic matter, carbon, heat or pollutants between the continental shelf and the deep sea (Ceramicola et al., 2015). These specific morphologies favor the generation of local complex hydrodynamic processes whose impact, interactions and relaxations have not been fully investigated due to the small scales involved and the laborious *in-situ* measurements. Understanding the circulation patterns in submarine canyons is a first step to characterize the interaction between hydrodynamic and sedimentary processes, benthic and pelagic habitat development, connectivity or contaminant transfer in canyons and slopes. It will also contribute to improving the representation of canyons in numerical models. In the northwestern sector of the Mediterranean Sea, the Gulf of Lions is one of the oceanic margins with the highest density of submarine canyons in the world with 3 to 4 canyons per 100 km (Allen and Durrieu de Madron, 2009; Würtz, 2012). The easternmost canyon of this area is the Cassidaigne submarine canyon (Figure 1).

While other canyons of the Gulf of Lions are sedimentary marine constructions (Mauffrey, 2015), the Cassidaigne submarine canyon is characterized by a steep, narrow and aerial morphology due to its particular origin (Ceramicola et al., 2015). During the Messinian salinity crisis, the level of the Mediterranean Sea was at least 1500 m lower than today (Gargani and Rigollet, 2007). As the head of the Cassidaigne canyon was exposed to the open air, it was initially eroded by winds and rivers before being further incised by currents after reflooding of the Mediterranean Sea. Unlike other canyons that gradually widen downstream, the Cassidaigne canyon of 6 km wide in its middle part is characterized by a narrowing of about 2 km wide at 1700 m depth downstream (Fabri et al., 2017). This specific morphology restricts and controls the local circulation. Fabri et al. (2017) identified maximum current velocities to the west part of the canyon head, but also at 1900 m depth at the canyon gorge and along its axis near the sea floor, in most confined areas with narrow morphologies.

The western part of the Gulf of Lions is well documented (Baztan et al., 2005; Jordi et al., 2005; Rennie, 2005; DeGeest et al., 2008; Lofi and Berné, 2008; Palanques et al., 2008; Ahumada-Sempoal et al., 2015) but the eastern region is not well known in terms of sedimentary geology. The Cassidaigne canyon is located in a microtidal area far from the Rhone, with negligible input of freshwater and sediments such as the karstic underwater flow coming from the Vallat des Brayes (Cavalera et al., 2010) and the discharge of the wastewater treatment plant of Cortiou near the surface (Oursel et al., 2014)). For 48 years, between 1967 and 2015, 30 megatons of red mud (bauxite residues) have been artificially discharged by the Gardanne plant at 400 m depth in the eastern canyon head (Alteo environnement Gardanne 2017 and Dauvin, 2009). The red mud flowed and spread along and across the canyon down to 2500 m depth. Although chemically inert, the remaining sediments cover the canyon bottom and act as flow tracers contributing to the characterization of hydrodynamic processes and sediment transport in the canyon. The interaction between sedimentary

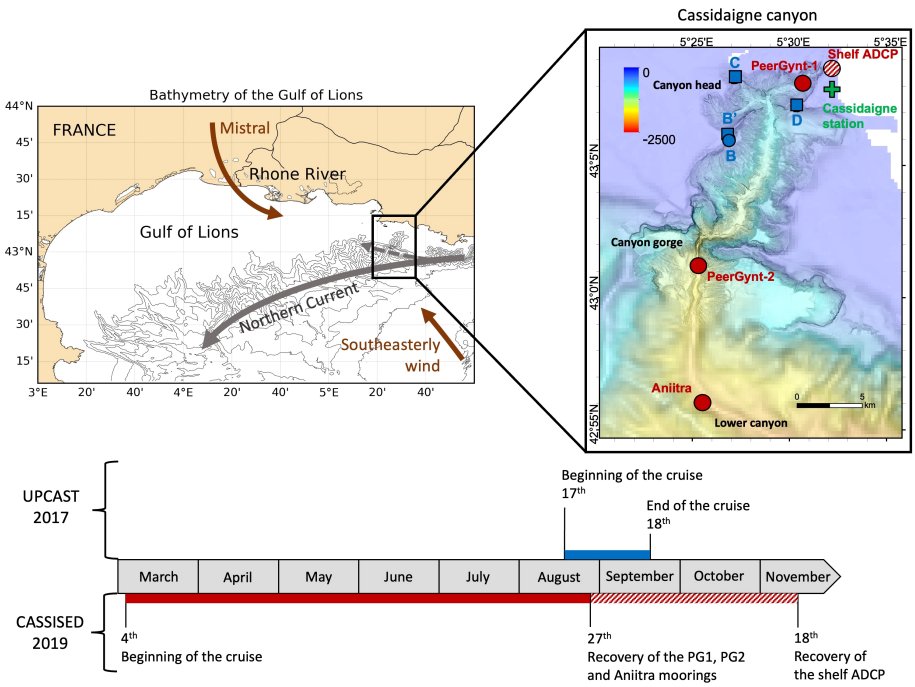


FIGURE 1
Bathymetry of the Gulf of Lions (top left), located between 42°N and 43.5°N of latitude and between 3°E and 6°E of longitude in the Mediterranean Sea, a semi-enclosed microtidal sea linked with the Atlantic Ocean by the Strait of Gibraltar. Its depth varies from 76 m on average on the shelf to 2500 m in the open sea. The gray arrow corresponds to the general circulation of the NC and the dashed gray arrow refers to its intrusion over the Gulf of Lions. Bathymetry of the Cassidaigne submarine canyon (m, right), the easternmost canyon in the Gulf of Lions, located 7 km away from the coast of Cassis. The squares refer to the position of the Mastodon-2d thermistor lines and the circles correspond to the ADCP current moorings for both UPCAST 2017 (in blue) and CASSISED 2019 (in red) cruises. Their deployment time is specified on the time lines (bottom). The green cross refers to the T-MedNet Cassidaigne station.

and hydrodynamic processes remains an open question. In most previous studies, the processes were analyzed separately.

Hydrodynamic processes in canyons such as upwelling or downwelling are relatively well known. Many studies were performed on the shelf or in idealized submarine canyons through numerical models and considering a simplified permanent forcing (She and Klinck, 2000; Kämpf, 2006; Allen and Durrieu de Madron, 2009; Saldías and Allen, 2020). The presence of submarine canyons incising the shelf modifies the structure of wind-induced upwellings and downwellings. In general, downwellings are characterized by down-canyon flows that tend to move away from the upstream edge of the canyon (i.e. the first edge met by the along-shore flow) and exit along the downstream edge (i.e. the last edge met by the along-shore flow). Upwellings are characterized by up-canyon flows along the upstream canyon rim and with an outflow of water masses on the downstream side (Allen and Durrieu de Madron, 2009). During an upwelling event, the flow crosses isobaths, stretching the water column and thus generating a cyclonic circulation within the canyon and an anticyclonic flow at the downstream edge (Hickey, 1997). Upwelling and downwelling can be separated into three phases: a time-dependent response of the water column to wind forcing, a non-linear established advection driven flow and consequently a relaxation phase (Allen and Durrieu de Madron, 2009). During the second phase, the response of the water column depends on its stratification and the canyon's morphology. Up to now, upwelling and downwelling have been mainly studied under stratified conditions. Studies on the Barkley and Astoria canyons demonstrated that non-linear terms and transient movements during set-up at short time scales within the canyon cause a break in the geostrophic balance, which is approximately in equilibrium on the shelf (Hickey, 1997; Allen et al., 2001; Allen and Hickey, 2010). Finally, the relaxation phase of upwelling and downwelling produces notable but less documented responses (Allen and Durrieu de Madron, 2009 and Hickey, 1997).

In the Gulf of Lions, upwellings are characterized by the movement of cold water from deeper levels to the surface. They lead to a drop of surface temperature in stratified conditions and a general increase in salinity in the water column (Millot, 1979; Millot, 1990; Odic et al., 2022 and Millot, 1997; Millot and Taupier-Letage, 2005). Upwellings are induced by westerly winds (Tramontane) and north-westerly winds (Mistral). The Mistral is characterized by intense (i.e. 25 m $s^{-1}$) episodes lasting several weeks in winter and weaker episodes (i.e. 10 to 15 m $s^{-1}$) during summer (Millot, 1990; Albérola and Millot, 2003; Millot, 2005 and Fabri et al., 2017). It generates six upwelling cells along the Gulf of Lions' margin, the strongest being close to the Cassidaigne canyon. Downwellings are induced by easterly winds. Both westerly and easterly winds' occurrence, speed and duration depend on the season. These winds blow in a succession of isolated storms generating transient movements and quasi-inertial oscillations (Petrenko, 2003). During fall, storm occurrence increases and upwellings and downwellings contribute to the homogenization of the water column (Fabri et al., 2017).

The Cassidaigne submarine canyon is also influenced by the Northern Current (NC), the northern branch of the general circulation in the northwestern Mediterranean Sea. It forms a surface slope current flowing from the Ligurian to the Catalan sea, characterized by a seasonal variability ranging from 1 m $s^{-1}$ in winter to 0.3 m $s^{-1}$ in summer (Conan and Millot, 1995; Flexas et al., 2002; Albérola and Millot, 2003; Petrenko, 2003; Guihou et al., 2013). The mesoscale variability of the NC manifests itself in the form of meanders which are particularly important in winter when it is the most unstable (Millot, 1997; Petrenko, 2003; Rubio et al., 2009). The NC usually flows along the shelf break front off the Gulf of Lions. During some south-easterly storms (Petrenko, 2003; Millot, 2005), intermittent Mistral's periods or relaxation of strong Mistral's events (Millot and Wald, 1980), up to 30% of its flow can separate from the main branch and enter the shelf mainly at the eastern entrance of the Gulf of Lions (Conan and Millot, 1995; Petrenko, 2003; Guihou et al., 2013) and potentially above the canyon (Pairaud et al., 2011). The impact of the NC on the water column has been mainly studied in the Grand-Rhone canyon (Durrieu de Madron, 1994 and Durrieu de Madron et al., 1999) or on the shelf (Rubio et al., 2009; Ross et al., 2016) but its interaction with the Cassidaigne canyon is not well documented. NC intrusion induces a vertical structure reorganization of the currents and a variation in surface temperature. Ross et al. (2016) studied the intrusion of the NC in the bay of Marseilles. The cold, nutrient-rich water brought to the surface during upwelling events is gradually replaced by warm, nutrient-poor water, in the observed 70 meters upper layer.

The variety and complexity of forcing processes around the Cassidaigne canyon implies taking into account their interaction and the transitions between regimes which are still not well-known in this region. The flow is forced both by the wind (generating upwelling, downwelling and inertia currents) and by the NC. It is also constrained by the seabed morphology. The knowledge of the Cassidaigne canyon area has been improved by previous oceanographic cruises (Pairaud et al., 2017; Danioux, 2018; Dennielou, 2019; Pairaud and Fuchs, 2021). In this paper, the shelf dynamics during strong upwelling events is analyzed using data gathered in 2017 over a period of 1 month. The behavior of residual currents on the shelf and within the canyon is analyzed with a second dataset collected in 2019 over a period of 6 to 8 months. The use of data from oceanographic campaigns allowed deepening the understanding of hydrodynamic and sedimentary processes in the Cassidaigne canyon. It also allowed the definition of a relevant study strategy. The paper is organized as follows: Section 2 introduces the materials and methods, i.e., the collection of *in-situ* and wind data and the data processing methods. Section 3 focuses on the main results considering periods of both non-stratified and stratified conditions. A focus on significant transient events (NC intrusions, upwellings) and occasional events (turbidity currents) is discussed in relation to previous studies in Section 4.

# 2 Materials and methods

## 2.1 Observations and modeling

Hydrological and hydrodynamic data were obtained during several monitoring periods (from 1 to 8 months) in and around the Cassidaigne canyon. Instruments were deployed along mooring lines

or mounted on benthic structures during two oceanographic cruises (Pairaud, 2017; Dennielou, 2019).

### 2.1.1 UPCAST 2017 campaign

In 2017, a one-month time-series of current and temperature data were acquired during the UPCAST 2017 oceanographic cruise from August 17$^{th}$ to September 18$^{th}$ 2017. The campaign was carried out in the northwestern Mediterranean Sea between the Calanques of Marseilles and the Hyéres islands (south of Toulon) on the RV Thetys II (Pairaud, 2017). The aim was to carry out physical and biogeochemical measurements to understand the interaction of the upwelling of Cassis with the local circulation in the Cassidaigne canyon and with the general circulation.

In addition to en-route measurements from the ship, a 300 kHz ADCP recording upward was moored on the shelf west of the canyon head at 125 m depth (B on Figure 1, Table 1). It was configured with a sampling rate of 10 min and measured currents in the water column from 8 to 108 m depth above the seabed using bins of 5 m size.

Three Mastodon-2d thermistor lines were deployed (Figure 1, Table 2, Figure S1): (i) on the shelf west of the canyon (B') at 125 m depth, (ii) at the canyon head (C) at 193 m depth and (iii) on the shelf east of the canyon (D) at 190 m depth. A Mastodon-2d thermistor line is a low-cost moored line (Lazure et al., 2015) used to record temperature and pressure along the water column. Pressure sensors were key to check the behavior of the line as it could be affected and bent by currents. It resulted in temperature measurements with a precision of 0.1°C.

### 2.1.2 CASSISED 2019 campaign

In the same area, the CASSISED oceanographic field experiment (Dennielou, 2019) was led from March 4$^{th}$ to August 30$^{th}$ 2019 (spring-summer). The aim of this campaign was to understand the transfer of particles from the continental shelf to the deep sea through the Cassidaigne canyon. The red mud injected in the canyon was considered as sediment flux tracers. The goal was also to estimate the

TABLE 1 Position and setting of each ADCP mooring used during the UPCAST 2017 and CASSISED 2019 cruises.

| Mooring | B | Shelf | PG1 | PG2 | Aniitra |
|---|---|---|---|---|---|
| **Deployment date** | 17 Aug 2017 | 4 March 2019 | 5 March 2019 | 5 March 2019 | 5 March 2019 |
| **Recovery date** | 18 Sept 2017 | 10 Nov 2019 | 26 Aug 2019 | 27 August 2019 | 27 Aug 2019 |
| **Latitude** | N43°06,2220 | N43°08,7780 | N43°08,2367 | N43°01,3409 | N42°56,1653 |
| **Longitude** | E5°26,8620 | E5°32,2440 | E5°30,7570 | E5°25,3316 | E5°25,5704 |
| **Depth of seabed (m)** | 125 | 86 | 422 | 1628 | 1906 |
| **Distance to seabed (m)** | 0 | 0 | 100 | 100 | 300 |
| **Ping frequency (kHz)** | 300 | 300 | 300 | 300 | 75 |
| **Sampling period (min)** | 10 | 15 | 10 | 10 | 10 |
| **Bin size (m)** | 5 | 4 | 4 | 4 | 4 |
| **Number of bins** | 24 | 20 | 24 | 19 | 72 |
| **Bin range from the seabed (m)** | 8-123 | 7-83 | 0-93 | 0-72 | 0-286 |
| **Number of pings per ensemble** | 50 | 50 | 60 | 60 | 60 |

TABLE 2 Position and setting of the thermistor lines and pressure and temperature sensors of each Mastodon-2d used during the UPCAST 2017 cruise.

| Mastodon-2d | B' | | | | | C | | | | | D | | | | |
|---|---|---|---|---|---|---|---|---|---|---|---|---|---|---|---|
| **Deployment date** | 17 Aug 2017 | | | | | 17 Aug 2017 | | | | | 17 Aug 2017 | | | | |
| **Recovery date** | 18 Sept 2017 | | | | | 18 Sept 2017 | | | | | 18 Sept 2017 | | | | |
| **Latitude** | N43°06,2096 | | | | | N43°08,453 | | | | | N43°07,3953 | | | | |
| **Longitude** | E5°26,8616 | | | | | E5°27,140 | | | | | E5°30,3355 | | | | |
| **Depth of seabed (m)** | 125 | | | | | 193 | | | | | 190 | | | | |
| **Sampling period (min)** | 5 | | | | | 5 | | | | | 5 | | | | |
| **Averaged vertical resolution (m)** | 12.71 | | | | | 15.01 | | | | | 20.18 | | | | |
| **Precision (°C)** | 0.1 | | | | | 0.1 | | | | | 0.1 | | | | |
| **Number of sensors** | 10 | | | | | 10 | | | | | 10 | | | | |
| **Mean sensors depth from the seabed (m)** | 0 | 9 | 18 | 29 | 43 | 0 | 10 | 25 | 44 | 69 | 0 | 10 | 24 | 50 | 75 |
| | 59 | 74 | 89 | 104 | 114 | 96 | 121 | 146 | 161 | 172 | 100 | 126 | 151 | 171 | 181 |

influence of upwellings, gravity currents and NC on particle movements with the aim of improving knowledge of the turbiditic channel, end lobes and contourites.

On the shelf, a 300 kHz ADCP looking upward, hereafter referred to as "shelf ADCP" (Figure 1, Table 1, Figure S1), was moored at 86 m bottom depth northeast of the canyon head. It sampled at a rate of 15 min part of the water column from 7 to 75 m depth above the seabed using bins of 4 m size. Due to a dysfunction of the acoustic release, this ADCP was recovered later on November 18$^{th}$ 2019. In the canyon, two 300 kHz ADCPs recording downward (PeerGynt moorings PG1 at the canyon head and PG2 embedded in the turbiditic channel at the outlet of the gorge) were immersed 100 m above the seafloor which was at 422 m depth for PG1 and 1628 m depth for PG2. They sampled at a rate of 10 min part of the water column from 13 to 93 m above the seabed and from 32 to 72 m depth above the seabed respectively using bins of 4 m size. A 75 kHz ADCP scanning downward (Aniitra mooring) was located 300 m above the 1906 m depth seafloor along the sedimentary ridge. It sampled at a rate of 10 min part of the water column using bins of 4 m size. The PG1 and PG2 moorings were equipped with STBD 6000 turbidimeters.

In deeper water layers, the measurements made by the 75 kHz Aniitra mooring were noisy. They had a lower resolution and velocity precision as they were configured to track turbidity currents, with higher speeds and particle charges than the background flows. Due to the ADCP configuration (4 m cell size), there was a high standard deviation in the data (0.047 m $s^{-1}$), which was of the order of magnitude of the measured velocity data. Data were often missing, especially at the beginning of the time series when too few particles were present in the water column. In the first half of the sampled water column, the nearest of the Aniitra mooring, the gaps were in the range of 10 to 30 min on average. The closer to the seabed, the more gaps in the data, sometimes of more than 24 h, resulting in very unreliable data. From March 5$^{th}$ to June 14$^{th}$, a lot of data were missing from the seabed to 198 m above the seabed. From June 15$^{th}$ to August 27$^{th}$, a lot of data were missing from the seabed to 149 m above the seabed. Therefore, only the upper part of the water column, from 198 to 269 m above the seabed, was exploited for the long-term residual current analysis. Moving means with a 30-minute window were first applied to the data to smooth the measurements and to reduce the noise in the velocity time series. Then, nearest-neighbor interpolations had to be carried out to fill isolated data gaps. This methodology generates a continuous time series but prevents from analyzing the signal at a period of less than 1 hour. Finally, the entire water column was analyzed for the turbidity current study.

Two temperature profiles in October 2019 were provided by the regional temperature observation network T-MEDNet (www.t-mednet.org) at the Cassidaigne station (43°08.740'N, 5°32.742'E, Figure 1) managed by Dorian Guillemain (MIO, Marseilles, France). Nine temperature sensors were attached to a rocky wall from 5 to 45 m depth. Data were acquired using temperature sensor HOBO Pro V2 Temp U22-001 (Accuracy ± 0.2°C).

### 2.1.3 Numerical models

The nearest meteorological station (Marignane airport) is separated from the canyon area by a remarkable orography (the Calanques massif) and is not sufficiently relevant in the area. In this approach, wind data were provided by the wind derived AROME (1.3 km resolution) modeling developed by the French Meteorological Office. The MARS3D (3D hydrodynamical Model for Applications at Regional Scale) model was used to simulate the coastal and regional circulation (developed by Lazure and Dumas, 2008; revised by Duhaut et al., 2008). For this study, the operational configuration "MENOR" of the MARS3D model (Garnier et al., 2014), which extends from the Balearic Islands to the Gulf of Lions and the Ligurian Sea (0°E 16°E, 39.5°N 44.5°N) was used. The model has a horizontal resolution of 1.2 km. The vertical resolution is defined using a generalized sigma coordinate system with 60 vertical levels on the order of ten centimeters near the surface, ten meters in the middle of the water column and a few meters near the bottom for a depth in the range of 200-1000 m.

## 2.2 Data processing strategy

### 2.2.1 Local circulation

The ADCP provided the zonal ($u$) and meridional ($v$) components of the horizontal velocity on a sampled portion of the water column. On the shelf, these velocities were analyzed considering a surface and a bottom layer separately. A characteristic surface layer depth of 65 ± 6 m has been defined empirically using either the thermocline depth or the current shear in order to best fit the observations. In order to do so, wind data were used together with current data (speed, stickplots…) provided by the shelf ADCPs and temperature data provided by the Mastodon-2d thermistor lines at all depths.

The non-stratified period was defined from March to early May, when Hovmöller diagrams showed a homogeneous water column (with almost the same current speed at the surface and the bottom) and temperature data were not characterized by important variations (of less than 0.2°C). In addition, the regional temperature observation network T-MEDNet showed an onset of stratification in early May.

The dynamical response to the offshore Ekman transport can produce a coastal upwelling. The horizontal fluxes deduced from the zonal and meridional components of the Ekman transport in steady state conditions were computed as:

$$U_{ek} = \frac{\tau_y}{\rho_e f} \quad (1)$$

$$V_{ek} = -\frac{\tau_x}{\rho_e f} \quad (2)$$

where $\rho_e$= 1025 kg $m^{-3}$ is the water volumetric mass and $f$=$10^{-4}$ rad $s^{-1}$ is the Coriolis parameter at the Cassidaigne canyon. $\tau_x$ and $\tau_y$ are the zonal and meridional component of the wind stress $\tau = \rho_a C_D \mathbf{U_{10}}^2$ where $\rho_a$=1.2 kg $m^{-3}$ is the air volumetric mass, $C_D$=1.5×$10^{-3}$ is the air-sea friction coefficient and $\mathbf{U_{10}}$ is the wind velocity at 10 m above the sea surface given by the AROME model.

In the canyon, the along-canyon $V_{along}$ and cross-canyon $V_{cross}$ velocities were calculated from $u$ and $v$. $V_{along}$ is positive up-canyon and $V_{cross}$ is positive to the west when looking up-canyon. The $V_{along}$ direction was determined by an angle α clockwise from north at each mooring in the canyon (PG1, PG2 and Aniitra from the CASSISED 2019 cruise): $\alpha_{PG1}$ = 22°, $\alpha_{PG2}$ = 357° and $\alpha_{Aniitra}$=322°. The Fourier transform of $V_{along}$ and $V_{cross}$ were calculated (S2).

### 2.2.2 Upwelling detection

To detect upwelling events, favorable westerly local winds were first identified using the meteorological model (Figure 2). In stratified conditions, upwellings were then characterized by a temperature decrease $\Delta T$ (Figure 2) on the shelf near the sea floor where ADCP temperature sensors were located. Comparison of wind and temperature variability allowed to determine the temperature drops associated with Mistral events. However, this method was less effective under non-stratified conditions. In this case, the ADCPs provided information on the current direction and shear. During upwelling events, the current was characterized by an offshore component near the surface and an onshore component near the sea floor.

To provide a quantitative analysis of the role of wind forcing in displacing water masses, the maximum current speed vertically averaged on the part of the water column measured by the ADCP was estimated for each upwelling event. It was related to the maximum wind speed.

### 2.2.3 Northern current intrusion

NC intrusions on the shelf were identified using operational results from the MARS3D MENOR and AROME models. Favorable southeast storms or Mistral's relaxation events were first identified using the meteorological model hindcasts. Then, a qualitative estimation of NC intrusion events was made by observing the direction of the surface currents from the MENOR forecasts. Finally, a quantitative estimation of these intrusions was performed following the approach described by Casella et al. (2020). This method is based on the evaluation of the onshore volume flux $F$ crossing through the 200 m isobath at eastern entrance of the Gulf of Lions. The flux is normalized:

$$F_n = \frac{F - \bar{F}}{\sigma_F} \quad (3)$$

where $\bar{F}$ is the temporal mean and $\sigma_F$ is the standard deviation of the flux, both evaluated over a 10-year period with 3-hourly model outputs. Considering the NC intrusion as an event of infrequent and strong intensity, a threshold of $F_n$>1 is considered to characterize it.

## 3 Results

### 3.1 Shelf circulation in the canyon area

Shelf circulation in the vicinity of the Cassidaigne submarine canyon is modulated by the wind, by the regional circulation and by its underlying complex morphology. Both surface and bottom currents may differ, depending on the stratification. The local shelf circulation is presented hereafter considering separately the surface and bottom water layers under non-stratified or stratified conditions.

### 3.1.1 Westerly wind-induced upwellings and consecutive transients

During the non-stratified period (from March to early May, CASSISED 2019 cruise), Mistral and south-easterlies alternated (Figure 3). Upwellings were found to require Mistral events of more than 18.3 ± 4 m $s^{-1}$ to be generated. During Mistral events, the shelf mooring north-east of the canyon (Figure 3) recorded 7 days of upwelling events in March and 11 days between April and early May. It led to a mean estimation of 9 days of upwelling per month. This short period of observation suggested a relatively high occurrence of upwelling under non-stratified conditions. Upwellings were

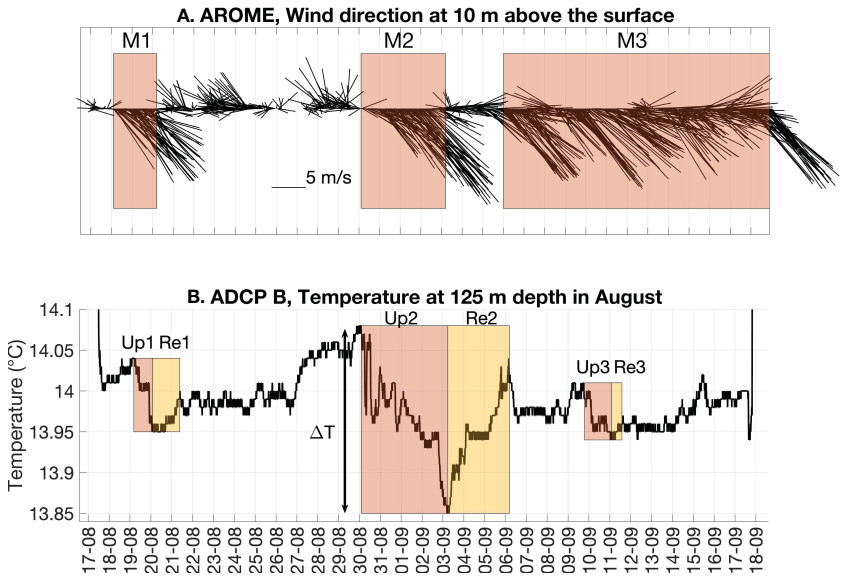


FIGURE 2
**(A)** Wind direction determined using the AROME meteorological model hindcasts during the UPCAST 2017 cruise. The stickplots point in the direction of the wind. Stickplots directed towards south-east to east (red boxes '*M1*', '*M2*' and '*M3*') correspond to Mistral events. **(B)** Temperature record (°C) measured at 125 m depth by the ADCP B (UPCAST 2017 cruise) under stratified conditions. Upwelling (red boxes '*Up1*', '*Up2*' and '*Up3*') generated by '*M1*', '*M2*' and '*M3*' respectively induce a decrease of temperature $\Delta T$ in the water column. Their corresponding relaxation '*Re1*', '*Re2*' and '*Re3*' are represented by the yellow boxes.

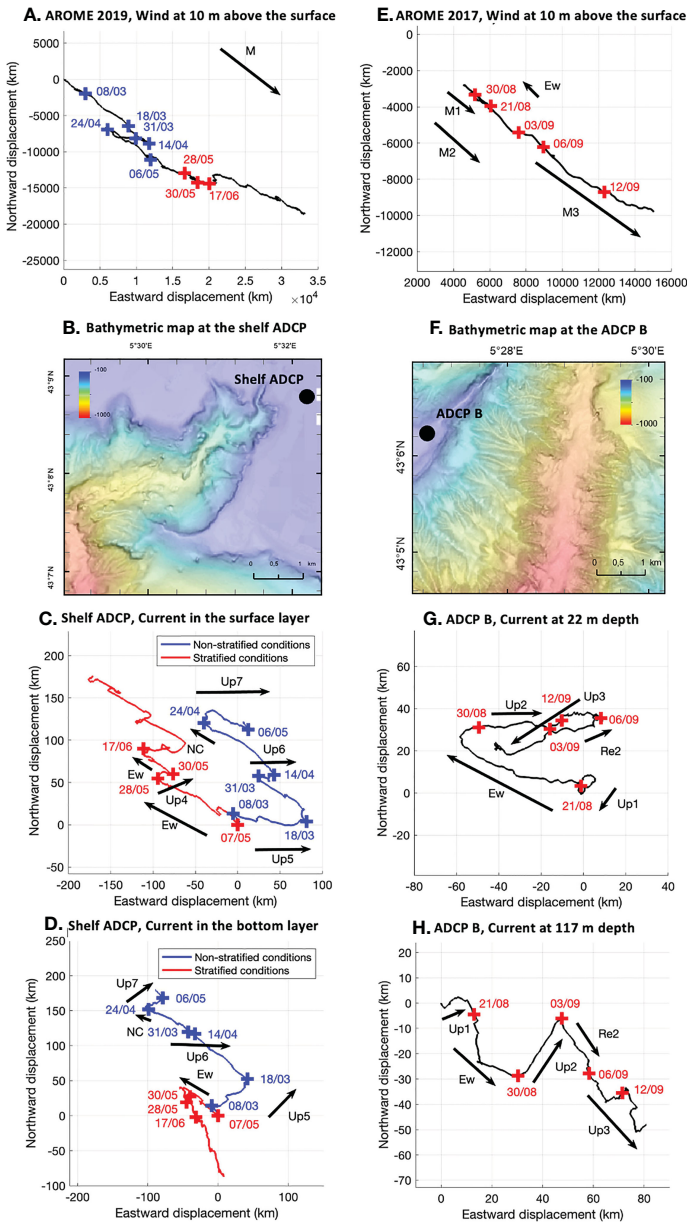


FIGURE 3
**(A)** Hodograph of the wind determined by the AROME meteorological model at 10 m above the surface during the CASSISED 2019 measurement period. '*M*' refers to the direction of the Mistral. **(B)** Bathymetric map at the shelf ADCP (m). Hodograph of the eulerian current measured by the shelf ADCP averaged on: **(C)** the surface layer of 65 m depth and **(D)** on the bottom layer. '*Up4*', '*Up5*', '*Up6*' and '*Up7*' correspond to upwelling events. '*Ew*' refers to easterly wind. '*NC*' corresponds to Northern Current intrusion. Blue crosses and lines refer to events in non-stratified conditions and red crosses and lines refer to events in stratified conditions. **(E)** Hodograph of the wind determined by the AROME meteorological model at 10 m above the surface during the UPCAST 2017 measurement period. '*M1*', '*M2*' and '*M3*' correspond to Mistral events. '*Ew*' refers to easterly wind. **(F)** Bathymetric map at the ADCP B (m). Hodograph of the eulerian current measured by the ADCP B: **(G)** at 22 m depth and **(H)** at 117 m depth. '*Up1*', '*Up2*' and '*Up3*' correspond to upwelling events. '*Re2*' is the relaxation phase of the '*Up2*' upwelling event.

represented on Figures 3C and D ('Up5', 'Up6' and 'Up7'). Upwellings were identified between the 8$^{th}$ and 18$^{th}$ of March (period 'Up5'). Other upwellings were identified between March 31$^{st}$ and April 14$^{th}$ (period 'Up6'). A last event was recorded between April 26$^{th}$ at 16:00 and May 6$^{th}$ at 06:00 (period 'Up7'). The surface layer (Figure 3) exhibited an eastward to southeastward (SE) direction of the current (i.e. along-shore) during Mistral events. Current speeds varied between 0.1 and 0.2 m s$^{-1}$. Near the seabed (Figure 4), the current direction was northeastward (NE, i.e. onshore) during upwelling events. Current speeds were in the range of 0.05 to 0.2 m s$^{-1}$. Thus, under non-stratified conditions, the wind controlled the circulation over almost the entire water column. Near the seabed, the current was also influenced by the presence of the Cassidaigne canyon further south, which orientated the flow NE along its axis.

While very few upwellings could be identified during the non-stratified period based on the temperature record at the shelf edge, they emerged clearly in the Hovmöller diagram of $v$ (Figure 4). The vertical shear of meridional (i.e., across-shore) current associated with the upwelling showed a 2-layer water column. The shearing interface was located between 40 and 70 m depth.

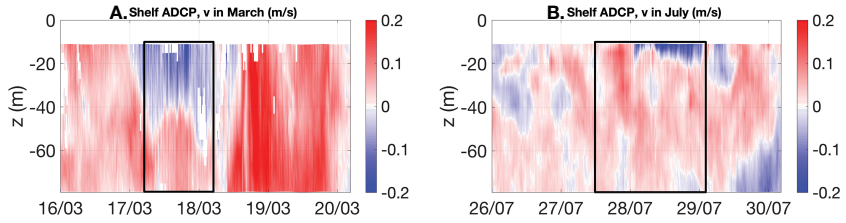


FIGURE 4
Meridional current (m $s^{-1}$) measured by the shelf ADCP: **(A)** in March and **(B)** in July. The boxes indicate upwelling events.

Under stratified conditions (from May to October), upwellings were observed for Mistral forcing of more than 14 m $s^{-1}$ both during the 2017 and 2019 cruises. 5 days per month of upwelling events were recorded on average. In August-September 2017, three strong Mistral events able to trigger upwelling occurred from August 18$^{th}$ to August 21$^{st}$, from August 30$^{th}$ to September 3$^{rd}$ and from September 6$^{th}$ till the end of the cruise ('M1', 'M2' and 'M3' on Figures 2, 3E). Over the same period, three upwellings have been identified on the shelf west of the canyon (Figure 3 and 'Up1', 'Up2' and 'Up3' on Figures 2, 3G, H). In particular, the 'Up3' upwelling was generated by the 'M3' Mistral event disrupted by short-time southerly wind pulses. It resulted in a temperature oscillation (Figure 2) on the shelf making it difficult to precisely identify the duration of the upwelling. It probably lasted more than 15 days. Thus, it was a particularly long phenomenon compared to other processes generally observed in the region.

Near the surface, currents on the shelf both west and northeast of the canyon orientated quickly to the wind direction during stratified conditions. Northeast of the canyon, currents were directed NE and varied between 0.1 and 0.2 m $s^{-1}$. West of the canyon, currents were either southwestward (SW, i.e. offshore, 'Up1' and 'Up3') or eastward (i.e. along-shore, 'Up2') and varied between 0.03 and 0.1 m $s^{-1}$. Near the bottom, the canyon impacts the local circulation. Northeast of the canyon, a SE residual current was recorded. It probably corresponded to an upwelling jet induced by an outflow from the eastern lobe of the canyon. Currents varied between 0.03 and 0.15 m $s^{-1}$. West of the canyon, the 'Up1' and 'Up2' upwelling events were characterized by a NE (i.e. onshore) current as a probable channelization of the flow in the vicinity of the canyon. Currents varied between 0.01 and 0.1 m $s^{-1}$. While current speeds were almost the same in the surface and the bottom layer in non-stratified conditions, they are weaker in the bottom layer in stratified conditions. The stratification restricts vertical mixing and hence the development of the Ekman Layer and the impact of wind in the bottom layer. The maximum contribution of upwelling processes to offshore surface layer velocity both to the west and to the northeast of the canyon can be evaluated using equations 1 and 2 in the range of 0.008 m $s^{-1}$. This result, estimated in a simplified case considering a constant wind, provides an estimate of magnitude of the current created by offshore winds. It is estimated to be negligible compared to the transient coastal currents generated by the wind.

Under stratified conditions, the shear pattern was not evident to detect as the offshore component of the current was confined in the surface mixed layer and was beyond the range of the ADCP (Figure 4). However, upwellings led to a drop in surface temperature (Figure 5). The most important temperature decrease was recorded during the 'Up2' upwelling event with a drop of 10°C at 11 m depth as found by Fabri et al. (2017) for a similar event in 2013.

Following an upwelling event under stratified conditions, the water column whose temperature initially decreased tends to warm up again to a threshold value. This transition phase is the relaxation from the upwelling. From the current hodographs (Figures 3G) and stickplots (Figures 5A), the currents reversed their direction from upwellings' active phase during the relaxation phase ('Re1', 'Re2' and 'Re3' on Figures 2, 3G, H, 5).

### 3.1.2 Easterly winds and NC intrusion events

In general, NC intrusion events are more frequent in autumn-winter than in spring-summer. In 2019, the MENOR model indicated an occurrence of 4 days per month of NC intrusion in stratified conditions and 9 days per month in non-stratified conditions as shown by Casella et al. (2020). NC intrusions occur under easterlies or during the relaxation of Mistral events. Near the surface, the northwestward (NW) direction of the current recorded by the shelf ADCP (CASSISED 2019) northeast of the canyon head was due either to easterlies or to NC intrusions ('Ew' and 'NC' on Figures 3C) both under stratified and non-stratified conditions. For example, a NC intrusion event 'NC' occurred on April 22$^{nd}$ 2019 (i.e. in non-stratified conditions) under easterlies. At the same time, the shelf ADCP recorded maximum current speeds of 0.41 m $s^{-1}$ at 14:00 in the surface layer and 0.4 m $s^{-1}$ at 23:00 in the bottom layer (not shown).

On October 24$^{th}$ (i.e. under stratified conditions), the strongest NC intrusion event observed in 2019 was recorded (Figure 6). This event occurred after a south-easterly storm of more than 15 m $s^{-1}$ from October 22$^{nd}$ to October 23$^{rd}$. The NC intrusion led to a supply of warm water at 86 m depth on the shelf leading to an increase of the temperature from 20 to 20.25°C near the surface and from 17.9 to 20.25°C at the deepest water layers (Figures 6B). This event also contributed to a homogenization of the current recorded along the 80 m depth of the water column at the measurement location (Figures 6D). The shelf ADCP recorded maximum current speeds of 0.36 m $s^{-1}$ at 12:00 in the surface layer and 0.3 m $s^{-1}$ at 14:00 in the bottom layer. NC intrusion events contributed to facilitate the vertical mixing even in stratified conditions.

## 3.2 Circulation inside the canyon

The CASSISED 2019 experiment provided a unique opportunity to study the currents in the deeper water layers along the canyon. Three locations were investigated: the canyon head, the canyon gorge

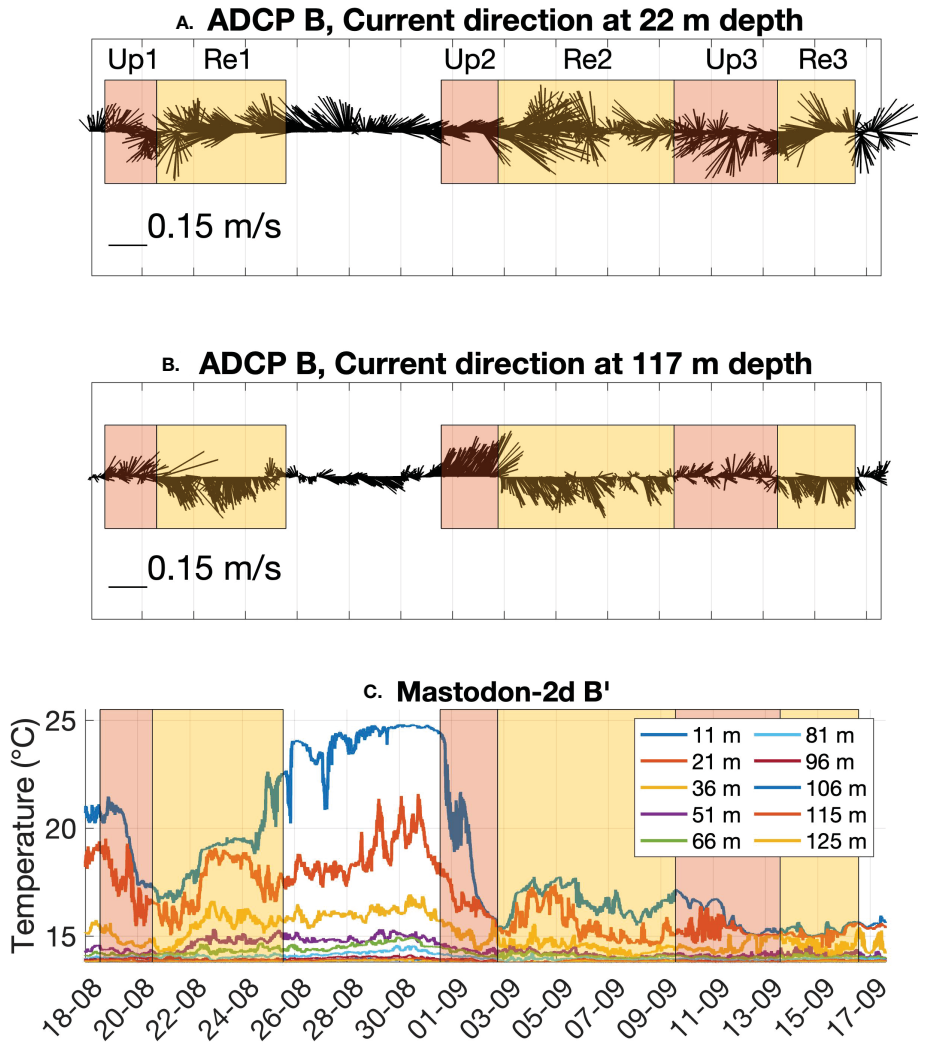


FIGURE 5
Current direction and speed measured by the ADCP B: **(A)** at 22 m depth and **(B)** at 117 m depth. The stickplots point in the direction of the current. **(C)** Temperature records (°C) measured by the Mastodon-2d B' thermistor line during the UPCAST 2017 cruise for each sensor. The red boxes '*Up1*', '*Up2*' and '*Up3*' correspond to upwelling events. The yellow boxes '*Re1*', '*Re2*' and '*Re3*' refer to the corresponding relaxation phases.

and the lower canyon. Averaged Eulerian hodographs were plotted at each location to evaluate the direction of residual currents and their fluctuations (Figure 7).

### 3.2.1 In the canyon head

The canyon head was studied using the PG1 mooring (from 13 to 93 m above the sea floor at 422 m depth, Figure 7, Table 1). It was located at the northeastern branch of the canyon head in a constrained area of about 1 or 2 km wide. Along-canyon currents $V_{along}$ ranged from 0.04 to 0.08 m $s^{-1}$. Cross-canyon currents $V_{cross}$ were slightly weaker and ranged from 0.03 to 0.06 m $s^{-1}$.

The orientation of the current was evaluated under non-stratified and stratified conditions (Figure 7). Under non-stratified conditions, a residual NW (i.e. cross-canyon) current was recorded. Under stratified conditions, the circulation was characterized by a residual northward current in May and an up-canyon residual NE (i.e. along-canyon) current during the rest of the measurement period. Finally, the high frequency components of the current were oriented in the same direction as the canyon axis. These results suggest that the local circulation at the canyon head is strongly dependent on the stratification. The current seemed to be mainly modulated by the general circulation or by oscillatory current under non-stratified conditions. Under stratified conditions, water masses movements were limited by the density differences between the surface and the seabed. Currents at the canyon head appeared to be mainly modulated by the canyon morphology, favoring an upward or downward along-canyon flow. It suggests that the canyon favors vertical mixing under stratified conditions.

The Fourier transform of $V_{cross}$ and $V_{along}$ (see Figures S2A, S2B) showed dominant peaks around 0.7 day period (17 h) under non-stratified conditions. The same result was obtained for $V_{along}$ under stratified conditions. The flow at the canyon head was strongly modulated by along-canyon near-inertial fluctuations as figured in Figures 7, 8A, B and on the $V_{along}$ averaged over the water column in March (Figure 9). This result is consistent with the findings of Flexas et al. (2002) on near-inertial currents at 240 m depth on the shelf. Conversely, $V_{cross}$ Fourier transform under stratified conditions

showed a clear peak at 2.6 days period, as a probable impact of the NC mesoscale activity (Conan and Millot, 1995; Flexas et al., 2002).

### 3.2.2 In the canyon gorge

The canyon gorge was studied using the PG2 mooring (from 32 to 72 m above the seafloor at 1628 m depth, Figure 7, Table 1). It was located in a 2 km wide narrowing area. A constant up-canyon component was recorded during the entire measurement period (Figure 7). It was generally reinforced during upwelling events (Figure 8). Under non-stratified conditions, residual currents were characterized by a NW displacement of 80 km in 2 months resulting in a residual current of about 0.015 m $s^{-1}$. Under stratified conditions, residual currents were weaker. They were marked by a NW displacement of about 100 km in 4 months resulting in a residual current of about 0.01 m $s^{-1}$. $V_{along}$ speed varied in the range 0.02 to 0.1 m $s^{-1}$.$V_{cross}$ speed varied in the range of 0.02 to 0.08 m $s^{-1}$. Then, residual currents under stratified conditions represented almost 10% of the $V_{along}$ and $V_{cross}$ transient oscillation amplitude.

At some short occasions, the mean flow was reversed and directed down-canyon during relaxation of strong upwellings (e.g. after April 15$^{th}$), south-easterlies (e.g. on August 5$^{th}$) or NC intrusions both in non-stratified and stratified conditions. During these events, SE currents were recorded by the PG2 mooring (zoom on Figure 7). This inversion of the flow was also observable on the along-canyon Hovmöller diagram shown in Figures 8C.

The Fourier transform analysis of $V_{cross}$ and $V_{along}$ (see Figures S2C, S2D) indicated similar results in non-stratified and stratified conditions. $V_{cross}$ was marked by dominant peaks of about 2.5 days period. $V_{along}$ was marked by dominant peaks of 5 to 6 days period. These results, combined with the $V_{along}$ averaged over the water column in March (Figure 9) suggested that the circulation at the canyon gorge was influenced by the general circulation (between 2 and 6 days period as mentioned by Flexas et al., 2002), near-diurnal oscillations (24 h, March 20$^{th}$ to March 24$^{th}$) or near-inertial fluctuations (17 h, March 8$^{th}$ to March 12$^{th}$). The signal at 24 h was less expected as the northern part of the Mediterranean Sea is generally referred to as a mixed semi-diurnal tidal regime.

### 3.2.3 In the lower canyon

The lower canyon was observed using the Aniitra mooring (from 198 to 269 m above the sea floor at 1906 m depth, Figure 7, Table 1). It was located along the canyon's sedimentary ridge where both $V_{along}$ and $V_{cross}$ currents were weaker than at shallower locations of other ADCPs (Figures 8E, F). Above the abyssal plain, the residual velocity was westward (Figure 7) in the range of 0.003 m $s^{-1}$ in non-stratified period and 0.004 m $s^{-1}$ in stratified period. Additionally, the velocity exhibited a strong variability, with NW (i.e. up-canyon) and SE (i.e., down-canyon) oscillations, partially constrained by the channel, both under non-stratified and stratified conditions. In detail, cycloidal patterns were present, suggesting the transit of eddies. In March and April, the area probably experienced cyclonic structures traveling westward while during summer weaker anticyclonic structures dominated. The turbulent mesoscale bottom circulation, characterized by these eddies,

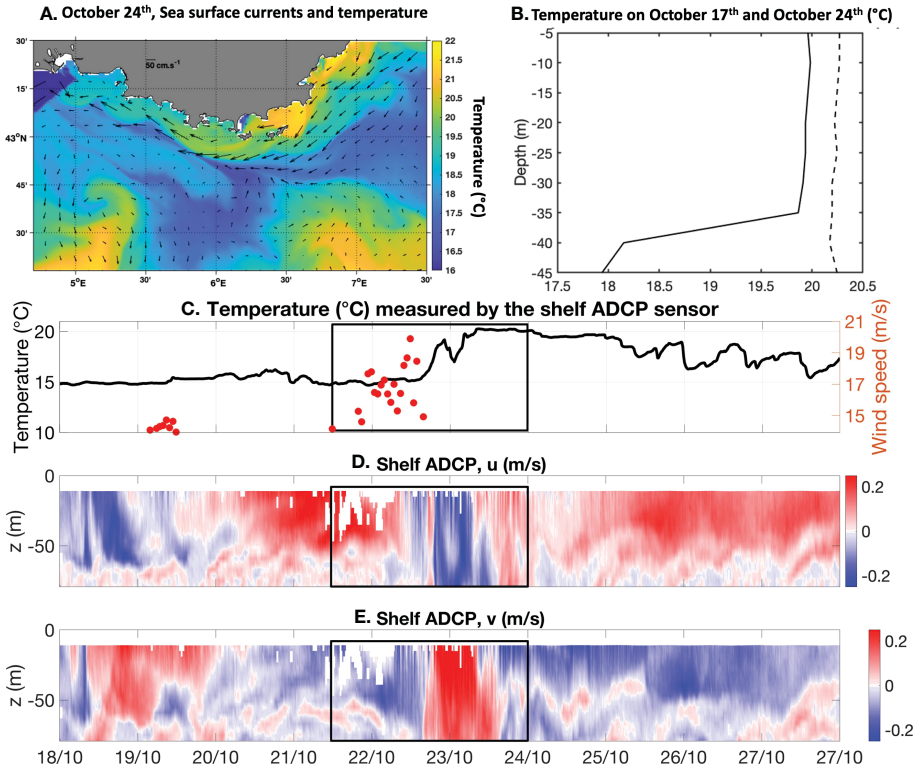


FIGURE 6
**(A)** Sea surface velocity currents (arrows) and temperature (°C, colors) estimated by the MARS3D MENOR 1200 model on October 24$^{th}$ 2019 at 12:00. **(B)** Temperature profiles measured by temperature sensors at the T-MedNet Cassidaigne station on October 17$^{th}$ at 12:00 (continuous line) before a NC intrusion over the Gulf of Lions and on October 24$^{th}$ at 12:00 (dashed line) during a NC intrusion over the Gulf of Lions. **(C)** Temperature (black line, °C) measured by the shelf ADCP at 86 m depth and wind speed (red dots) estimated by the AROME meteorological model. An easterly storm of more than 15 m $s^{-1}$ started on October 22$^{nd}$ 2019, inducing a NC intrusion event from October 23$^{rd}$ to October 24$^{th}$ 2019. **(D)** Zonal and **(E)** meridional currents (m $s^{-1}$) measured by the shelf ADCP (CASSISED 2019) from October 18$^{th}$ to October 28$^{th}$. Both the easterly storm and the NC intrusion event are included in the boxes.

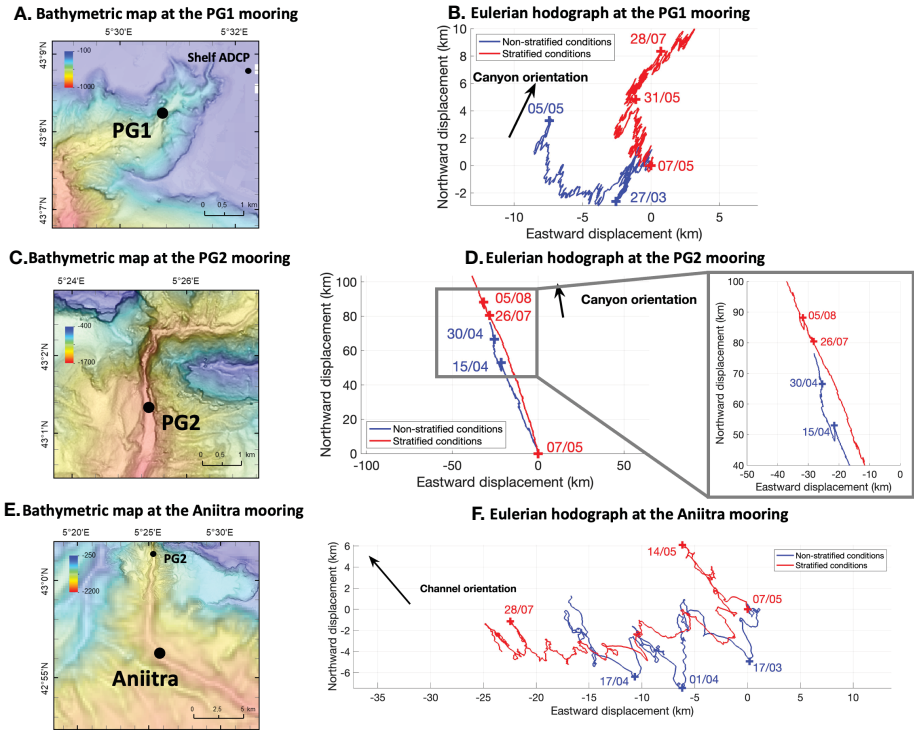


FIGURE 7
**(A)** Bathymetric map at the PG1 mooring (m). **(B)** Hodograph of the eulerian mean velocity in the bottom layer measured by the PG1 mooring. **(C)** Bathymetric map at the PG2 mooring (m). **(D)** Hodograph of the eulerian mean velocity in the bottom layer measured by the PG2 mooring and zoom on some inversion of the current direction. **(E)** Bathymetric map at the Aniitra mooring (m). **(F)** Hodograph of the eulerian mean velocity in the bottom layer measured by the Aniitra mooring. Blue lines and crosses correspond to non-stratified conditions. Red lines and crosses correspond to stratified conditions.

did not affect the rest of the canyon as there were no such fluctuations on the hodograph at PG2 (Figure 7).

The Fourier transform analysis of $V_{cross}$ and $V_{along}$ (see Figures S2E, S2F) indicated dominant peaks of 3 to 6 days period. Thus, the circulation along the canyon's sedimentary ridge is mainly influenced by the regional circulation.

## 3.3 Extreme events

From March 9$^{th}$ at 05:00 to March 11$^{th}$ 2019 at 19:00, an upwelling associated with maximum current's intensities of 0.21 m s$^{-1}$ on the shelf was forced by a Mistral event of 17.4 m s$^{-1}$. During the relaxation of the upwelling, on March 11$^{th}$ at 19:00, the turbidimeter

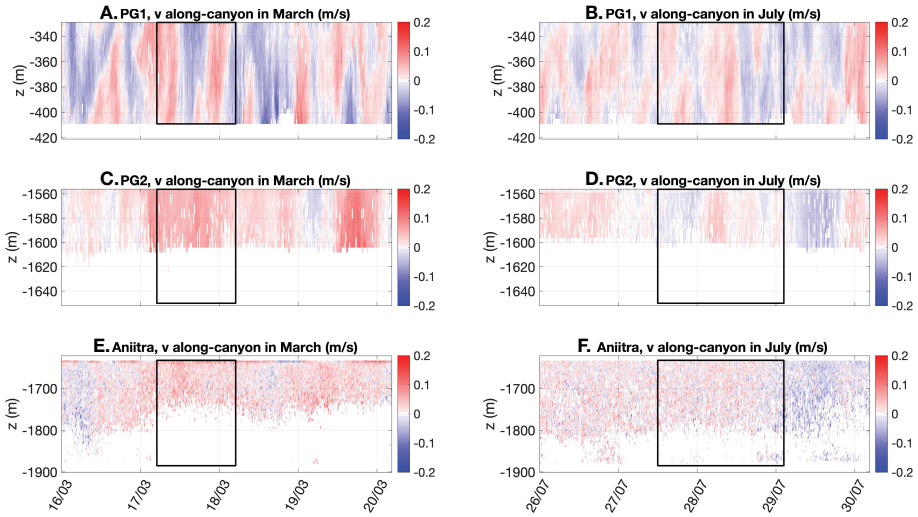


FIGURE 8
Along-canyon current (m s$^{-1}$) measured by the PG1 mooring: **(A)** in March and **(B)** in July. Along-canyon current (m s) measured by the PG2 mooring: **(C)** in March and **(D)** in July. Along-canyon current (m s$^{-1}$) measured by the Aniitra mooring: **(E)** in March and **(F)** in July. The boxes indicate upwelling events.

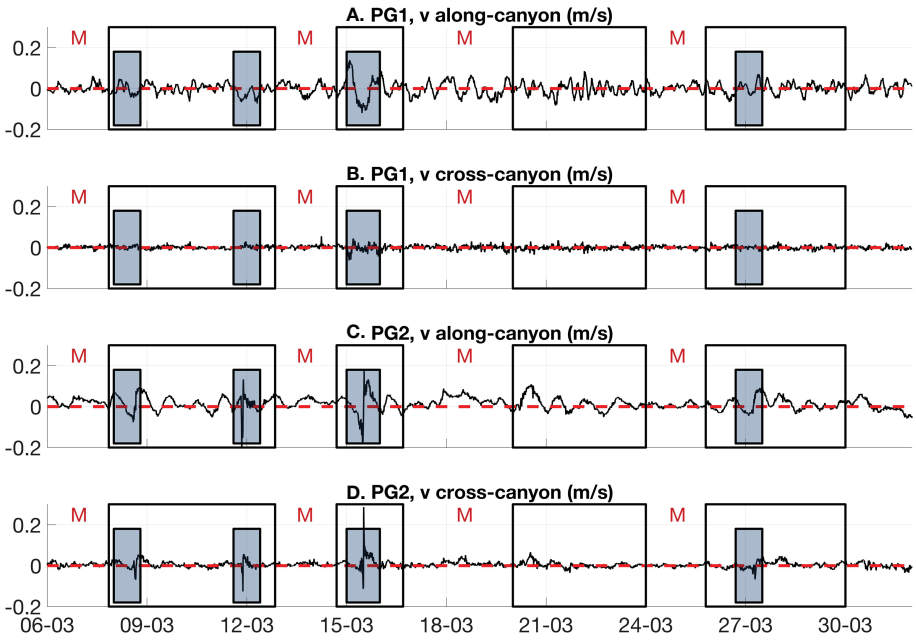


FIGURE 9
Averaged **(A)** along-canyon and **(B)** cross-canyon currents (m $s^{-1}$) measured by the PG1 mooring in March. Averaged **(C)** along-canyon and **(D)** cross-canyon currents (m $s^{-1}$) measured by the PG2 mooring in March. The filled gray boxes refer to specific events. The black boxes correspond to the relaxation of Mistral events. '*M*' refers to Mistral events occurring over the periods preceding the boxes.

at the canyon head (PG1) did not record any significant event but the turbidimeter at the gorge outlet (PG2) measured a turbid event of 760.5 NTU (Figure 10). The echo intensity signal of the ADCP at PG2 was also strongly affected (Figure 10), revealing a signal characterized by particle entrainment near the sea floor and suspended particles around 1580 m depth for about 20 h from the start of the event. The vertically averaged along-channel current ($V_{along}$, Figure 9, Table 3) on the bottom layer at the canyon gorge was characterized by a maximum downward velocity of -0.2 m $s^{-1}$ followed immediately by a weaker upward velocity in the range of 0.15 m $s_{-1}$. A similar pattern was also observed on the cross-channel current ($V_{cross}$, Figure 9, Table 3) with a decrease reaching -0.13 m $s^{-1}$ (i.e. eastward) followed immediately by an increase reaching 0.06 m $s^{-1}$ (i.e. westward). This turbid event was also detected 6 hours later on the backscatter signal of the deeper Aniitra mooring (Figure 10). As the PG2 and Aniitra moorings were separated by about 11.33 km, the sediment front flowed with a mean velocity of about 0.52 m $s^{-1}$ (Figures 10C).

From March 13$^{th}$ at 07:00 to March 16$^{th}$ at 08:00, another upwelling associated with a maximum current speed of 0.34 m $s^{-1}$ was recorded on the shelf during a Mistral event of 19.8 m $s^{-1}$. On March 15$^{th}$ at 12:00, a turbid event of lower intensity (turbidity of 5 NTU) was recorded at PG2 (Figures 10F). This event was associated with strong along-canyon and

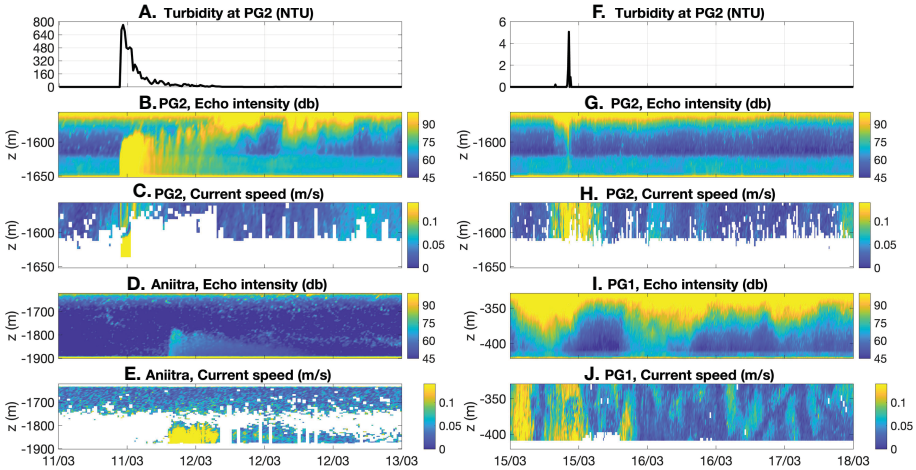


FIGURE 10
From March 11th to March 13th: **(A)** Turbidity (NTU), **(B)** echo intensity (db) and **(C)** current speed (m s-1) measured by the PG2 mooring and **(D)** echo intensity (db) and **(E)** current speed (m s-1) measured by the Aniitra mooring. From March 15th to March 18th: **(F)** Turbidity (NTU), **(G)** echo intensity (db) and **(H)** current speed (m s-1) measured by the PG2 mooring and **(I)** echo intensity (db) and **(J)** current speed (m s-1) measured by the PG1 mooring.

cross-canyon velocities (Figures 9C, Table 3). The $V_{along}$ velocity was first marked by a decrease reaching -0.18 m $s^{-1}$ (i.e. down-canyon) from March 15$^{th}$ at 00:00 to March 15$^{th}$ at 12:00 and then by an increase reaching 0.17 m $s^{-1}$ (i.e. up-canyon). The $V_{cross}$ velocity was characterized by a more important oscillation with a decrease reaching -0.14 m $s^{-1}$ (i.e. eastward direction), and then an increase reaching 0.296 m $s^{-1}$ (i.e. westward direction). An event of strong currents was also recorded on March 15$^{th}$ at 02:00 by the PG1 mooring (Figures 9, 10J). The $V_{along}$ velocity was first marked by an increase reaching 0.12 m $s^{-1}$ (i.e. up-canyon) from March 14$^{th}$ at 17:00 to March 15$^{th}$ at 02:00 and then by a decrease reaching -0.12 m $s^{-1}$ (i.e. down-canyon) until March 15$^{th}$ at 11:00. Although no turbid event was measured by the turbidimeter of PG1, unlike at PG2, the $V_{along}$ velocities measured at the canyon head and gorge (Figures 9A) indicated a co-occurring hydrodynamic process. Moreover, the PG1 backscatter signal experienced high variability in the upper part of the water column (Figure 10). These signals might correspond to suspended particles coming from the shelf and oscillating at near-inertial frequencies in the canyon at the PG1 mooring location, which was found to be mainly influenced by wind forcing (section 3.2.1).

During these two turbid events, both $V_{along}$ and $V_{cross}$ of PG2 were characterized by hourly peaks (Figures 9C).$V_{along}$ and $V_{cross}$ showed a few other velocity pulses that lasted up to one hour. As the sampling rate was 10 min, these peaks were not associated with noise signals. Such an isolated and short time scale event do not correspond to a purely hydrodynamic process. It suggests an interaction with the sedimentary movements despite an increase in the associated turbidity which remained much lower than for the extreme event of March 11$^{th}$.

# 4 Discussion

## 4.1 Residual circulation in the canyon

On the shelf, the current direction in the vicinity of the Cassidaigne canyon head is forced by westerly and easterly winds. It coincides with the wind direction on the entire water column in non-stratified conditions and on the surface layer in stratified conditions (Figure 3). This result complements observations made by Albérola and Millot (2003) in stratified conditions, highlighting the relation of current to wind direction. The wind is able to generate along-shore currents whose direction may induce upwelling or downwelling event in canyons. Previous simulations and numerical approaches compiled by Klinck (1996) emphasized the asymmetry of the geostrophic imbalance effect regarding the along-shore current direction. A left-bounded along-shore current (i.e., southeastward over the Cassidaigne canyon during the Mistral) generates an upward movement in the canyon. Conversely, a right-bounded current (i.e., northwestward during south-easterly winds) contributes to a downward motion in the canyon. On the shelf northeast of the Cassidaigne canyon head near the sea floor and at the canyon head, the along-shore northwestward (i.e., cross-canyon) residual current dominates from March to April, resulting in a weak and vanishing residual downward circulation. During summer, the bottom flow on the shelf northeast of the canyon head is directed southeastward, resulting in an up-canyon (i.e. northeastward) dynamics at the canyon head (Figures 3C , Figures 7A).

At the canyon gorge at 1600 m depth, currents are characterized by a quasi-permanent up-canyon flow both in non-stratified and stratified conditions (Figures 7C). Previous numerical experiments in idealized canyons led by Allen et al. (2001); Kämpf (2006) and Klinck (1996) explained this up-canyon flow as a geostrophic adjustment to barotropic pressure gradient when the current direction is opposed to the Kelvin waves propagation. Thus, having up-canyon flows at the canyon gorge in stratified conditions was expected. The narrow morphology of the Cassidaigne canyon induces a break in the geostrophic balance producing an unbalanced cross-shore (i.e. northeastward) pressure gradient, as mentioned by Allen et al. (2001), which favors up-canyon flows both in non-stratified and stratified conditions. Moreover, the quasi-permanent up-canyon flow observed at the canyon gorge suggests that upward flows can be extrapolated to the canyon body and contrasts with the observations made by Durrieu de Madron (1994), who noticed a dominant down-canyon flow in the Grand-Rhone canyon, due to the right-bounded NC flow. As upwellings are associated with upward movement of water masses, this observation suggests that upwelling may occur in the entire Cassidaigne canyon, from 1600 m depth to the shelf. This result complements numerical analysis led by Kämpf (2006) on an idealized canyon. Kämpf (2006) identified upwellings in most areas of the canyon generating a channeled up-canyon flow from up to 400 m depth onto the shelf. Moreover, Hickey (1997) mentioned a maximum upwelling phase characterized by a permanent up-canyon flow in the full Astoria canyon.

## 4.2 Transient upwelling and downwelling

Mistral events of more than 15 m $s^{-1}$ in speed generate multiple transient upwellings in the Cassidaigne canyon. Upwellings induce temperature decrease at the surface of up to 10°C (Figure 5). These results agree with the observations made by Hickey (1997) in the Astoria submarine canyon. The author noticed the generation of maximum upwellings, characterized by minimum temperature above the canyon rim, during stronger large-scale left-bounded along-shore winds. First, Hickey (1997) defined a transitory phase characterized by an increasing upwelling inducing a cyclonic flow in the canyon. In our study, there is a lack of data in the inner part of the Cassidaigne

TABLE 3 Maximum current speeds (m $s^{-1}$) recorded on the shelf and maximum along-canyon $V_{along}$ and cross-canyon Vcross speeds (m $s^{-1}$) recorded at the canyon gorge during two turbid events on March 11$^{th}$ and March 15$^{th}$.

| Current speeds on March 11$^{th}$ (m $s^{-1}$) | | | | | Current speeds on March 15$^{th}$ (m $s^{-1}$) | | | | |
|---|---|---|---|---|---|---|---|---|---|
| Shelf | PG2-$V_{along}$ | | PG2-$V_{cross}$ | | Shelf | PG2-$V_{along}$ | | PG2-$V_{cross}$ | |
| | Down-canyon | Up-canyon | Eastcanyon | Westward | | Down-canyon | Up-canyon | Eastcanyon | Westward |
| 0.21 | -0.2 | 0.15 | -0.13 | 0.06 | 0.34 | -0.18 | 0.17 | -0.14 | 0.296 |

canyon to observe the possible deep cyclonic dynamics generated by the stretching of the tube vortex under an upwelling-prone onshore current, as modeled by Kämpf (2006). A numerical modeling of the Cassidaigne canyon at high resolution, using both realistic and idealized cases (bathymetry, forcing) will contribute to the understanding of the impact of hydrodynamic processes on the local circulation of the canyon. It should be noticed that the time scale involved in such processes (e.g. five days for She and Klinck (2000)) and the narrowness of the canyon gorge do not favor the establishment of this characteristic pattern. Second, on the shelf northeast of the Cassidaigne canyon head, a SE trend of the bottom current was recorded under stratified conditions (Figure 3). The separation of the bottom layer from the surface layer results in the generation of a baroclinic upwelling jet, as mentioned by Saldías and Allen, 2020 and Allen et al., 2001. Finally, Hickey (1997) characterized upwelling's relaxation phase by an inversion of the current and a down-canyon flow, as observed in this study (Figures 3G, Figures 5A).

This study showed the dependence of upwelling and downwelling response on stratification and wind direction and speed, both seasonally variable, and the role of upwellings in vertical mixing by bringing cold water to the surface. As stated by Fraysse et al. (2013), from an ecological point of view, upwellings also contribute to the development of benthic and pelagic ecosystems in the canyon. Depending on their duration and associated speed, upwellings contribute to a supply of nutrients at the head of the canyon and can induce phytoplankton blooms.

Even though many studies have already been carried out on upwelling and downwelling in submarine canyons, the *in-situ* measurements conducted in the Cassidaigne canyon bring new information in a regional context, from the shelf at 86 m depth to the deep sea at 1906 m depth. However, the lack of data in non-stratified conditions does not allow to entirely characterize upwelling and downwelling processes in the Cassidaigne canyon. In a global context, these results emphasize the key role of submarine canyons in the generation of small-scale and mesoscale cross-shelf processes that interact with the along continental margin circulation. Depending on the time scales, the strength of the dynamics and the characteristics of the advected material, transport can be upward or downward in canyons. The morphology of submarine canyons is key in the modulation of local bottom circulation. Submarine canyons promote vertical mixing between the deep sea and the continental shelf during upwelling and downwelling events.

## 4.3 Inertial oscillations

The local circulation in and around the Cassidaigne canyon is modulated by wind forcing. Currents in the canyon head are marked by near-inertial fluctuations around 350 m depth (Figures 8A, Figure 9, Figure S2). In most of the literature, inertial currents were studied on the shelf break under atmospheric forcing (Pollard, 1970; Millot and Crépon, 1981; Font et al., 1995; Flexas et al., 2002; Gonella, 1971 and Petrenko (2003)). Flexas et al. (2002) studied the circulation on the shelf edge and the continental slope off Marseilles. They found more important near-inertial fluctuations at the shelf break than on the shelf at 240 m depth. The borders of the narrow and steep Cassidaigne canyon may favor near-inertial current fluctuations. Under stratified conditions, Petrenko (2003) and Millot and Crépon (1981) observed the generation of two-layer baroclinic inertial currents in the Gulf of Lions under strong wind forcing. Font et al. (1995) also noticed the repeated presence of clockwise current at the near-inertial frequency in the NC at 100 m depth. However, near-inertial fluctuations are observed at the canyon head both under non-stratified and stratified conditions. As the Cassidaigne canyon is located in a microtidal area, the inertia is an important component of the dynamics in the canyon. Unexpectedly, intermittent near-inertial fluctuations are also observed in the along-canyon currents at the canyon gorge, around 1600 m depth (Figure 9, Figure S2). Observation of inertial motion at such depth suggests that the wind also has an impact on the deeper water layers. As the canyon gorge is narrower (almost 2 km width) than the canyon body (almost 6 km width), the Cassidaigne canyon guides and amplifies the inertial waves towards the deep sea inducing stronger flows.

## 4.4 Northern current intrusion

Near the surface, NC intrusions favor a NW direction of the current on the shelf northeast of the canyon head both under non-stratified and stratified conditions with a seasonally variable occurrence and duration (Figures 3C). This result is similar to the findings by Fabri et al. (2017), who identified NW currents on the eastern part of the shelf around the Cassidaigne canyon due to NC intrusions. The Fourier transform at the canyon head and gorge and near the seabed, revealed the presence of peaks between 2 and 6 days periods which correspond to mesoscale and synoptic variability of the NC as observed by Sammari et al. (1995); Flexas et al. (2002) and Conan and Millot (1995). Near the sea floor, the local circulation may also be influenced by the propagation of bottom topographic Rossby waves characterized by periods longer than 2.5 days, as mentioned by Sammari et al. (1995). In contrast to the circulation in the Grand-Rhone canyon described by Durrieu de Madron (1994; 1999), the NC has a sporadic influence on the Cassidaigne canyon circulation and does not drive downward residual currents but only short lived ones. In addition, during NC intrusion events over the Gulf of Lions, the lower end of the upper Cassidaigne canyon is characterized by a narrowing, preventing any partial intrusion of the NC in the canyon as observed for the other canyons of the Gulf of Lions (Petrenko, 2003).

In a global context, submarine canyons are ubiquitous on continental margins. Residual circulation, transient dynamics and extreme events are all involved in the transport of carbon, heat, nutrients or micro-plastics between the shelf and the deep sea. Submarine canyons are expected to play a key role in the global circulation and in the generation of hydrodynamic processes. The results obtained in the Cassidaigne canyon emphasized an interaction between the canyon and the general circulation, modulated by the canyon's morphology.

## 4.5 Turbidity current

During the CASSISED 2019 cruise, two turbidity currents were directly observed for the first time at the canyon gorge on March 11$^{th}$ and March 15$^{th}$ (Figure 10). They both occurred during the relaxation

of upwelling events suggesting an interaction between hydrodynamic and sedimentary processes. Even if there is an average up-canyon flow at the canyon gorge, upwelling events tend to reinforce the current speed. They also favor a down-canyon flow during their relaxation, carrying away the sediments to the deep sea. According to Fabri et al. (2017), particles require currents of 0.2 to 0.4 m $s^{-1}$ to be resuspended. At the canyon gorge, along-canyon and cross-canyon currents recorded during these two turbidity currents could reach maximum values between 0.1 and 0.3 m $s^{-1}$ (Table 3) as modelled by Kämpf (2006). Thus, upwelling events occurring at the Cassidaigne canyon are able to move the local sediment in the canyon. The regional circulation may also be able to modify and control the movement of particles near the seabed. Results previously mentioned demonstrated an impact of NC intrusions or bottom Rossby topographic waves near the sea floor.

The turbidity current observed on March 11$^{th}$ is relatively short-lived (2 h at PG2) and propagates with a low velocity of 0.52 m $s^{-1}$ which is comparable to peak velocities observed for flood induced turbidity current in the Mediterranean Var canyon (Heerema et al., 2022). A stronger (1.5 m $s^{-1}$) and short-lived (6 min) turbidity current was observed under dilute river plume conditions by Hage et al. (2019). As shown by Talling et al. (2022) in the Congo submarine canyon, extreme turbidity events may reach propagations of up to 5 to 8 m $s^{-1}$. Even if relatively weak, the turbidity current generated in the Cassidaigne canyon under wind relaxation is able to effectively transport sediment stocked in the canyon to the deep sea in an upwelling dominated environment.

The western Gulf of Lions is marked by recurrent dense water cascading events during winter (Estournel et al., 2003 and Ulses et al., 2008) which could also occur in the Cassidaigne canyon. However, the Cassidaigne canyon is located in a small shelf area, which is not favorable to the generation of dense water cascading. The vicinity of the NC inhibits the formation of dense cold water east of the Gulf of Lions and upwelling events are also unfavorable to the accumulation of dense water near the coast.

In a global context, this paper demonstrated that sedimentary processes can be triggered by hydrodynamic processes controlling local sediment transport near the seabed. As submarine canyons are sediment-rich morphologies, the likely link between internal sedimentary and hydrodynamic processes in the Cassidaigne submarine canyon could be extended to other canyons. Fonnesu et al. (2019) found that the bottom circulation will rework the deposits and the transport of the sediments previously brought by turbidity currents in submarine canyons in a general context.

## 5 Conclusion

The Cassidaigne submarine canyon is located in an active circulation area where water masses are modulated by the wind, the regional circulation and the bottom morphology. The eastern Gulf of Lions is marked by recurrent westerly and easterly winds. On the one hand, south-easterly winds or Mistral's relaxation may favor right-bounded along-shore current, associated with down-canyon flows and NC intrusion events over the Gulf of Lions. NC intrusions lead to a homogenization of the water column in the vicinity of the Cassidaigne canyon. On the other hand, Mistral events of more than 14 m $s^{-1}$ generate left-bounded along-shore current associated with up-canyon flows.

Upwellings are observable throughout the canyon until 1600 m depth. They lead to strong transient dynamics and upwelling-relaxation cycles which are characterized by down-canyon counter currents. In the presence of the canyon, upwelling events promote vertical mixing between the deep sea and the continental shelf by bringing cold water to the surface. In addition, the increase in bottom currents during transients appears to be strong enough to resuspend particles and trigger extreme events such as turbidity currents. This highlights the forcing of sedimentary processes by hydrodynamic processes in submarine canyons.

The Cassidaigne canyon has an atypical morphology that modulates the local circulation. On the shelf near the bottom, the canyon morphology leads to a channelization of the flow under stratified conditions. It also orientates currents in the canyon head under stratified conditions and at the canyon gorge and along the sedimentary ridge independently of the stratification. Both the canyon head and gorge are marked by near-inertial fluctuations. Moreover, the circulation at the canyon gorge, observed for the first time, is characterized by a constant up-canyon flow, stronger under non-stratified conditions, and by near-diurnal oscillations. Unlike other canyons that gradually widen toward the seabed, the Cassidaigne canyon is characterized by a narrow constricting gorge. Thanks to this restricted outlet, a local amplification of currents allowed the observation of quasi-inertial waves in the deep part of the canyon. The canyon acts as a near-inertial wave-trap and downwards guide for the oscillations generated at the surface by the wind.

The observations carried out in the Cassidaigne canyon show the important role of canyons on both local and regional circulation. This knowledge will contribute to improve the understanding of sedimentary processes in the bottom layer, the characterization of benthic and pelagic habitats or the understanding of exchanges between the shelf and the seabed. It will also contribute to improving the representation of submarine canyons in numerical models and thus to deepen their study.

## Data availability statement

The raw data supporting the conclusions of this article are available as: Brun Lenaig, Pairaud Ivane, Silva Jacinto Ricardo, Garreau Pierre, Dennielou Bernard (2023). Hydrodynamic dataset from the UPCAST and CASSISED campaigns in the Cassidaigne canyon (NW Mediterranean Sea). SEANOE. https://doi.org/10.17882/92820.

## Author contributions

IP carried out the UPCAST 2017 cruise and BD, IP, and RS carried out the CASSISED 2019 cruise. BD realized the bathymetric maps. LB analyzed the data, interpreted the results, designed the figures and wrote the manuscript with critical feedback and help to shape the analysis and the manuscript from all authors. Previous processing of the data were led by IP and RS. All authors contributed to the article and approved the submitted version.

## Funding

Ifremer funded the PhD of LB.

## Acknowledgments

The authors acknowledge the technical team of the French Oceanographic Fleet (FOF) and the crews of the R/V THETYS II and R/V L'EUROPE for their contribution to the field experiments. The authors also thank Valérie Garnier, Christophe Ravel, Deny Malengros and Christel Pinazo for their help during the UPCAST campaign and Ronan Apprioual, Mikaël Roudaut and Jérémie Gouriou for the mooring deployments during the CASSISED cruise.

## Conflict of interest

The authors declare that the research was conducted in the absence of any commercial or financial relationships that could be construed as a potential conflict of interest.

## Publisher's note



## Supplementary material

The Supplementary Material for this article can be found online at: https://www.frontiersin.org/articles/10.3389/fmars.2023.1078831/full#supplementary-material

## References

Ahumada-Sempoal, M. A., Flexas, M. M., Bernardello, R., Bahamon, N., Cruzado, A., and Reyes-Hernández, C. (2015). Shelf-slope exchanges and particle dispersion in blanes submarine canyon (NW Mediterranean sea): A numerical study. *Continental Shelf Res.*, 109:35–45. doi: 10.1016/j.csr.2015.09.012

Albérola, C., and Millot, C. (2003). Circulation in the French mediterranean coastal zone near Marseilles: the influence of wind and the northern current. *Continental Shelf Res.* 23, 587–610. doi: 10.1016/S0278-4343(03)00002-5

Allen, S. E., and Durrieu de Madron, X. (2009). A review of the role of submarine canyons in deep-ocean exchange with the shelf. *Ocean Sci.* 5, 607–620. doi: 10.5194/os-5-607-2009

Allen, S. E., and Hickey, B. M. (2010). Dynamics of advection-driven upwelling over a shelf break submarine canyon. *J. Geophys Res.* 115. doi: 10.1029/2009JC005731

Allen, S., Vindeirinho, C., Thomson, R., Foreman, M., and Mackas, D. (2001). Physical and biological processes over a submarine canyon during an upwelling event. *Can. J. Fisheries Aquat. Sci.* 58, 671–684. doi: 10.1139/cjfas-58-4-671

Alteo environnement Gardanne, A. E (2017). *Gestion/réduction/arrêt*. https://alteo-environnement-gardanne.fr/-Gestion-Reduction-Arret-

Baztan, J., Berné, S., Olivet, J. L., Rabineau, M., Aslanian, D., Gaudin, M., et al. (2005). Axial incision: The key to understand submarine canyon evolution (in the western gulf of lion). *Mar. Petroleum Geology* 22, 805–826. doi: 10.1016/j.marpetgeo.2005.03.011

Casella, D., Meloni, M., Petrenko, A. A., Doglioli, A. M., and Bouffard, J. (2020). Coastal current intrusions from satellite altimetry. *Remote Sens.* 12, 3686. doi: 10.3390/rs12223686

Cavalera, T., Gilli, E., Mamindy-Pajany, Y., and Marmier, N. (2010). Mechanism of salt contamination of karstic springs related to the messinian deep stage. the speleological model of port miou (France). *Geodynamica Acta* 23, 15–28. doi: 10.3166/ga.23.15-28

Ceramicola, S., Amaro, T., Amblas, D., Cağatay, N., Carniel, S., Chiocci, F. L., et al. (2015). Submarine canyon dynamics - executive summary (Monaco: CIESM publisher), vol. 47 of. *CIESM Monograph.*, 47:7–20.

Conan, P., and Millot, C. (1995). Variability of the northern current off Marseilles, western Mediterranean Sea, from February to June 1992. *Oceanologica Acta* 18, 193–205.

Danioux, N. (2018). *2017 French oceanographic cruises report - bilan des campagnes océanographiques francaises 2017 (Ifremer)*. doi: 10.13155/55723 https://archimer.ifremer.fr/doc/00446/55723/

Dauvin, J.-C. (2009). Towards an impact assessment of bauxite red mud waste on the knowledge of the structure and functions of bathyal ecosystems: The example of the cassidaigne canyon (north-western Mediterranean Sea). *Mar. pollut. Bull.* 60, 197–206. doi: 10.1016/j.marpolbul.2009.09.026

DeGeest, A., Mullenbach, B., Puig, P., Nittrouer, C., Drexler, T., Durrieu de Madron, X., et al. (2008). Sediment accumulation in the western gulf of lions, France: The role of cap de creus canyon in linking shelf and slope sediment dispersal systems. *Continental Shelf Res.* 28, 2031–2047. doi: 10.1016/j.csr.2008.02.008

Dennielou, B. (2019). *CASSISED 2019 - 1-3 cruise, L'Europe R/V*. doi: 10.17600/18000904 https://campagnes.flotteoceanographique.fr/campagnes/18000904/

Duhaut, T., Honnorat, M., and Debreu, L. (2008). *Développements numériques pour le modèle MARS*. https://mars3d.ifremer.fr/content/download/49831/file/2008_05_30_INRIA_debreu_final.pdf

Durrieu de Madron, X. (1994). Hydrography and nepheloid structures in the grand-rhône canyon. *Continental Shelf Res.* 14, 457–477. doi: 10.1016/0278-4343(94)90098-1

Durrieu de Madron, X., Radakovitch, O., Heussner, S., Loye-Pilot, M., and Monaco, A. (1999). Role of the climatological and current variability on shelf-slope exchanges of particulate matter: Evidence from the rhône continental margin (NW Mediterranean). *Deep Sea Res. Part I: Oceanographic Res. Papers* 46, 1513–1538. doi: 10.1016/S0967-0637(99)00015-1

Estournel, C., Durrieu de Madron, X., Marsaleix, P., Auclair, F., Julliand, C., and Vehil, R. (2003). Observation and modeling of the winter coastal oceanic circulation in the gulf of lion under wind conditions influenced by the continental orography (FETCH experiment). *J. Geophys Res: Oceans* 108, 8059. doi: 10.1029/2001JC000825

Fabri, M.-C., Bargain, A., Pairaud, I., Pedel, L., and Taupier-Letage, I. (2017). Cold-water coral ecosystems in cassidaigne canyon_ an assessment of their environmental living conditions. *Deep-Sea Res. II* 137, 436–453. doi: 10.1016/j.dsr2.2016.06.006

Flexas, M., Durrieu de Madron, X., Garcia, M., Canals, M., and Arnau, P. (2002). Flow variability in the gulf of lions during the MATER HFF experiment (March–may 1997). *J. Mar. Syst.* 33-34, 197–214. doi: 10.1016/S0924-7963(02)00059-3

Fonnesu, M., Palermo, D., Galbiati, M., Bonamini, E., and Bendias, D. (2019). A new world-class deep-water play-type, deposited by the syndepositional interaction of turbidity flows and bottom currents: The giant Eocene coral field in northern Mozambique. *Mar. Petroleum Geology* 111, 179–201. doi: 10.1016/j.marpetgeo.2019.07.47

Font, J., Garcia-Ladona, E., and Gorriz, E. G. (1995). The seasonality of mesoscale motion in the northern current of the western Mediterranean: several years of evidence. *Oceanologica Acta* 18, 207–219.

Fraysse, M., Pinazo, C., Faure, V., Fuchs, R., Lazzari, P., Raimbault, P., et al. (2013). Development of a 3D coupled physical-biogeochemical model for the marseille coastal area (NW Mediterranean sea): What complexity is required in the coastal zone? *PloS One*, 18. doi: 10.1371/journal.pone.0080012

Gargani, J., and Rigollet, C. (2007). Mediterranean Sea Level variations during the messinian salinity crisis. *Geophys Res. Lett.* 34. doi: 10.1029/2007GL029885

Garnier, V., Pairaud, I. L., Nicolle, A., Alekseenko, E., Baklouti, M., Thouvenin, B., et al. (2014). MENOR: a high-resolution (1.2 km) modeling of the north-western mediterranean sea routinely run by the previmer operational forecast system. *Mercator Ocean Quaterly Newslett.* 49.

Gonella, J. (1971). A local study of inertial oscillations in the upper layers of the ocean. *Deep-Sea Res.* 18, 775–788. doi: 10.1016/0011-7471(71)90045-3

Guihou, K., Marmain, J., Ourmières, Y., Molcard, A., Zakardjian, B., and Forget, P. (2013). A case study of the mesoscale dynamics in the north-Western Mediterranean Sea: a combined data–model approach. *Ocean Dynamics* 63, 793–808. doi: 10.1007/s10236-013-0619-z

Hage, S., Cartigny, M., Summer, E., Clare, M., Clarke, J., Talling, P., et al. (2019). Direct monitoring reveals initiation of turbidity currents from extremely dilute river plumes. *Geophys Res. Lett.* 46, 11310–11320. doi: 10.1029/2019GL084526

Heerema, C., M.J.B., C., Silva Jacinto, R., Simmons, S., Apprioual, R., and Talling, P. (2022). How distinctive are flood-triggered turbidity currents? *J. Sedimentary Res.* 92, 1–11. doi: 10.2110/jsr.2020.168

Hickey, B. M. (1997). The response of a steep-sided, narrow canyon to time-variable wind forcing. *J. Phys. Oceanogr* 27, 697–726. doi: 10.1175/1520-0485(1997)027<0697:TROASS>2.0.CO;2

Jordi, A., Orfila, A., Basterretxea, G., and Tintoré, J. (2005). Shelf-slope exchanges by frontal variability in a steep submarine canyon. *Prog. Oceanogr* 66, 120–141. doi: 10.1016/j.pocean.2004.07.009

Kämpf, J. (2006). Transient wind-driven upwelling in a submarine canyon: A process-oriented modeling study. *J. Geophys Res.* 11. doi: 10.1029/2006JC003497

Klinck, J. M. (1996). Circulation near submarine canyons: A modeling study. *J. Geophys Res.* 101, 1211–1223. doi: 10.1029/95JC02901

Lazure, P., and Dumas, F. (2008). An external-internal mode coupling for a 3d hydrodynamical model for applications at regional scale (mars). *Adv. Water Resour.* 31, 233–250. doi: 10.1016/j.advwatres.2007.06.010

Lazure, P., Le Berre, D., and Gautier, L. (2015). Mastodon mooring system to measure seabed temperature data logger with ballast, release device at European continental shelf. *Sea Technol.* 56 (10), 19–21.

Lofi, J., and Berné, S. (2008). Evidence for pre-messinian submarine canyons on the gulf of lions slope (Western Mediterranean). *Mar. Petroleum Geology* 25, 804–817. doi: 10.1016/j.marpetgeo.2008.04.006

Mauffrey, M.-A. (2015). *Impact des variations du climat et du niveau marin sur les canyons sous-marins du golfe du lion (France) et de la marge de l'Ebre (Catalogne) au cours du plio-quaternaire* (UniversitÃ© de Perpignan, via Domitia). Ph.D. thesis. https://hal.science/tel-01300859/

Millot, C. (1979). Wind induced upwellings in the gulf of lions. *Oceanologica Acta* 2, 261–274.

Millot, C. (1990). The gulf of lions' hydrodynamics. *Continental Shelf Res.* 10, 885–894. doi: 10.1016/0278-4343(90)90065-T

Millot, C. (1997). Circulation in the Western Mediterranean Sea. *J. Mar. Syst.* 20, 423–442. doi: 10.1016/S0924-7963(98)00078-5

Millot, C. (2005). Circulation in the Mediterranean Sea: evidences, debates and unanswered questions. *Scientia Marina* 69, 5–21. doi: 10.3989/scimar.2005.69s15

Millot, C., and Crépon, M. (1981). Inertial oscillations on the continental shelf of the gulf of lions - observations and theory. *J. Phys. Oceanogr* 11, 639–657. doi: 10.1175/1520-0485(1981)011<0639:IOOTCS>2.0.CO;2

Millot, C., and Taupier-Letage, I. (2005). Circulation in the Mediterranean Sea. *Handb. Environ. Chem.* 5, 29–66. doi: 10.1007/b107143

Millot, C., and Wald, L. (1980). The effect of mistral wind on the ligurian current near provence. *Oceanologica Acta* 3, 399–402.

Odic, R., Bensoussan, N., Pinazo, C., Taupier-Letage,, and Rossi, V. (2022). Sporadic wind-driven Upwelling/Downwelling and associated Cooling/Warming along northwestern Mediterranean coastlines. *Continental Shelf Res.* 250 doi: 10.1016/j.csr.2022/104843

Oursel, B., Garnier, C., Pairaud, I., Omanovic, D., Durrieu, G., Syakti, A. D., et al. (2014). Behaviour and fate of urban particles in coastal waters: Settling rate, size distribution and metals contamination characterization. *Estuarine Coast. Shelf Sci.* 138, 14–26. doi: 10.1016/j.ecss.2013.12.002

Pairaud, I. (2017). *UPCAST oceanographic cruise, Thétys II R/V*. doi: 10.17600/17009500 https://campagnes.flotteoceanographique.fr/campagnes/17009500/

Pairaud, I., and Fuchs, R. (2021). *Rapport des campagnes TURBIDENT Leg1 (Mai 2018) et Leg2 (Octobre 2018)*. doi: 10.13155/78596 https://archimer.ifremer.fr/doc/00674/78596/

Pairaud, I., Garnier, V., Ravel, C., Berre, D. L., Leizour, S., and Lazure, P. (2017). "Mastodon-2D deployment in Mediterranean Sea during upcast field experiment," in *Mongoos workshop "Mediterranean Sea observing system"*(Athens, Greece).

Pairaud, I., Gatti, J., Bensoussan, N., Verney, R., and Garreau, P. (2011). Hydrology and circulation in a coastal area off marseille: Validation of a nested 3D model with observations. *J. Mar. Syst.* 88, 20–33. doi: 10.1016/j.jmarsys.2011.02.010

Palanques, A., Guillén, J., Puig, P., and Durrieu de Madron, X. (2008). Storm-driven shelf-to-canyon suspended sediment transport at the southwestern gulf of lions. *Continental Shelf Res.* 28, 1947–1956. doi: 10.1016/j.csr.2008.03.020

Petrenko, A. A. (2003). Variability of circulation features in the gulf of lion NW Mediterranean sea. importance of inertial currents. *Oceanologica Acta* 26, 323–338. doi: 10.1016/S0399-1784(03)00038-0

Pollard, R. T. (1970). On the generation by winds of inertial waves in the ocean. *Deep-Sea Res.* 17, 795–812. doi: 10.1016/0011-7471(70)90042-2

Rennie, S. J. (2005). *Oceanographic processes in the Perth canyon and their impact on productivity* (Curtin University of Technology). Ph.D. thesis. https://espace.curtin.edu.au/handle/20.500.11937/1904

Ross, O., Fraysse, M., Pinazo, C., and Pairaud, I. (2016). Impact of an intrusion by the northern current on the biogeochemistry in the eastern gulf of lion, NW Mediterranean. *Estuarine Coast. Shelf Sci.* 170, 1–9. doi: 10.1016/j.ecss.2015.12.022

Rubio, A., Tailandier, V., and Garreau, P. (2009). Reconstruction of the mediterranean northern current variability and associated cross-shelf transport in the gulf of lions from satellite-tracked drifters and model outputs. *J. Mar. Syst.* 78, S63–S78. doi: 10.1016/j.jmarsys.2009.01.011

Saldías, G., and Allen, S. (2020). The influence of a submarine canyon on the circulation and cross-shore exchanges around an upwelling front. *J. Phys. Oceanogr* 50, 1677-1698. doi: 10.1175/JPO-D-19-0130.1

Sammari, C., Millot, C., and Prieur, L. (1995). Aspects of the seasonal and mesoscale variabilities of the northern current in the western Mediterranean Sea inferred from the PROLIG-2 and PROS-6 experiments. *Deep-Sea Res.* 42, 893–917. doi: 10.1016/0967-0637(95)00031-Z

She, J. M., and Klinck, J. (2000). Flow near submarine canyons driven by constant winds. *J. Geophys Res: Oceans* 105, 28671–28694. doi: 10.1029/2000jc900126

Talling, P., Baker, M., Pope, E., Ruffell, S., Silva Jacinto, R., Heijnen, M., et al. (2022). Longest sediment flows yet measured show how major rivers connect efficiently to deep sea. *Nat. Commun.* 13. doi: 10.1038/s41467-022-31689-3

Ulses, C., Estournel, C., Bonnin, J., Durrieu de Madron, X., and Marsaleix, P. (2008). Impact of storms and dense water cascading on shelf-slope exchanges in the gulf of lion (NW Mediterranean). *J. Geophys Res.* 113. doi: 10.1029/2006JC003795

Würtz, M. (2012). *Mediterranean Submarine canyons: Ecology and governance* (Gland, Switzerland and Malaga, Spain: IUCN).